Interfacial energy analysis of supersonic particle impact adhesion conditions at the critical velocity

Kando H. Moonga[1,*] and Tienchien Jen[2]

[1]Department of Mechanical Engineering; University of Zambia ORCID: 0000-0001-9130-4090
[2]Department of Mechanical Engineering Science; University of Johannesburg ORCID: 0000-0003-1743-4668
[*]Corresponding author: khmoonga@unza.zm

Abstract

The critical velocity for adhesion of a microparticle on impact with a substrate is formulated and internal dynamics that lead to critical points are graphically illustrated. The modelling involves energy balance; kinetic, plastic and heat. Analysis of interfacial high strain-rate, the plastic equivalent strain and duration of plastic deformation brings out the internal material dynamics that lead to the critical point for material jetting at the particle substrate interface. Through non-dimensional analysis, the critical velocity is a point where plastic flow velocities, exceed acoustic flow velocities. This illustration may underpin underlying thermal transport and vibrational signatures in microparticle impacts.

Keywords: ballistic impact-adhesion, structural impact-excitation, heat transport, high strain rate, critical velocity, erosive wear, wave propagation, acoustics

1 Introduction

When a microparticle hits a target surface, it may rebound, adhere or erode from the surface. Ballistic impacts of microparticles are a key manufacturing process in short peening (Al-Obaid, 1995) and additive methods (Wang et al., 2023). Supersonic impacts of dust storms involving microparticles must be mitigated in aerospace vehicle structures to minimise changes in the dynamics and structural properties such as surface friction and surface roughness and eventual structural damage (Palmieri and Lambert, 2001); the need for mitigation of wear damage. Supersonic impact bonding only occurs at a certain velocity range which has been termed window of deposition (Schmidt et al., 2006). This velocity range is bounded by the critical velocity (minimum velocity) and the erosion velocity (maximum velocity) (Alkhimov et al., 1994; Moridi et al., 2013; Hassani-Gangaraj et al., 2018a; Li et al., 2006). Below the critical velocity the plastic deformation is too low to cause bonding whereas above the erosion velocity hydrodynamic penetration leads to strong erosion. Between these two characteristic velocities optimum conditions for deposition are reached (Schmidt et al., 2006). Both the critical and erosion velocity are characterized by spray material, powder properties, particle and substrate temperature (Wang et al., 2023; Chaban et al., 2021) and particle size (Dowding et al., 2020). Due to the small size of the particles, the interface physics maybe governed by microscopic heat transport, there is therefore a need for a careful study so as to inform the computational modelling approach including material constitutive methods Rahmati and Ghaei (2014) and the experimental interrogation methods.

2 Methods

2.1 Solution procedures

Analysis of the solution procedures were based on the implementation details in the Abaqus solver as detailed in the user manual in (Simulia, 2012). Computational models used are shown in Figure 1. The material parameters for this study are listed in Table 1. The details of the numerical modelling were first given in a doctoral thesis (Moonga, 2019) by the first author, some parts repeated here to make this paper

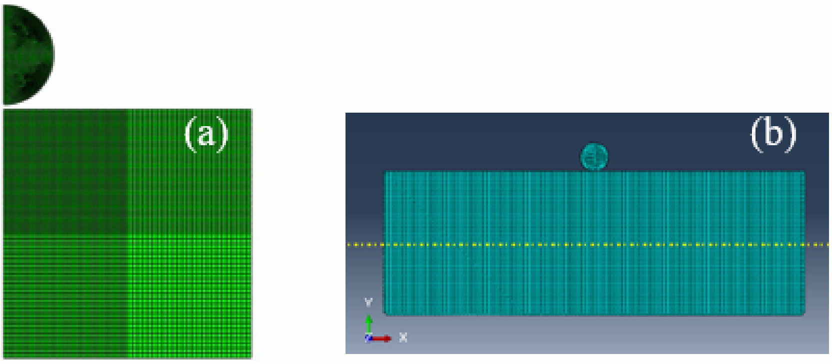

Figure 1: Computational model (a) 20µm particle diameter copper, (b) 10µm particle diameter copper on copper substrate with infinity boundaries on the sides and bottom surfaces.

self-contained. The general heat equation solved, equation 1, is an

$$\frac{\partial}{\partial x}\left(k\frac{\partial T}{\partial x}\right)+\frac{\partial}{\partial y}\left(k\frac{\partial T}{\partial y}\right)+\frac{\partial}{\partial z}\left(k\frac{\partial T}{\partial z}\right)+Q=\rho c\frac{\partial T}{\partial t} \tag{1}$$

energy conservation equation that applies Fourier's law $q_x=-k\frac{\partial T}{\partial x}$, $q_y=-k\frac{\partial T}{\partial y}$ and $q_z=-k\frac{\partial T}{\partial z}$ as the heat conduction components in the x, y, and z directions and k is the thermal conductivity. Q is internal heat generation per unit volume, ρ is the material density, c the specific heat capacity of the material, $\frac{\partial T}{\partial t}$ is the rate of change of temperature, $\frac{\partial T}{\partial z}$ is the directional temperature gradient.

In adiabatic analysis the increase in temperature is calculated directly at the material integration points based on adiabatic thermal energy increase caused by inelastic deformation (Simulia, 2012). Adiabatic analysis assumes there is no heat conduction during the material deformation. This assumption can be assumed to hold in short durations of high speed manufacturing processes involving large inelastic strains. When both inelastic generation and heat conduction are required, a fully coupled temperature-displacement analysis must be performed using fully coupled thermal-stress analysis (Simulia, 2012). Plastic straining gives rise to a heat flux per unit volume of

$$Q^{pl}=\beta\sigma_y\frac{d\varepsilon^{pl}}{dt}=\beta\sigma\dot{\varepsilon}^{pl} \tag{2}$$

where Q^{pl} is the heat flux (generation) that is added into the thermal energy balance, β is the user-specified material dependent inelastic heat generation fraction, σ is the stress, and $\dot{\varepsilon}^{pl}$ is the rate of plastic straining. In an adiabatic analysis the heat equation solved at each integration point is therefore given as

$$\rho c\frac{\partial T}{\partial t}=\beta\sigma_y\frac{d\varepsilon^{pl}}{dt} \tag{3}$$

where ρ is the material density and C is the specific heat which could also be temperature dependent. Equation 3 is directly obtained from equation 1 where the heat conduction components q_x, q_y and q_z are zero; and Q is defined by equation 2. Whereas when both inelastic generation and heat conduction are required the heat equation solved will be given by equation 1.

$$\frac{\partial}{\partial x}\left(k\frac{\partial T}{\partial x}\right)+\frac{\partial}{\partial y}\left(k\frac{\partial T}{\partial y}\right)+\frac{\partial}{\partial z}\left(k\frac{\partial T}{\partial z}\right)+\beta\sigma_y\frac{d\varepsilon^{pl}}{dt}=\rho c\frac{\partial T}{\partial t} \tag{4}$$

2.2 Mathematical modeling of critical points

All the mathematical modeling were based on the analysis of energy balance with interest at the particle substrate interface around the critical and erosion velocity.

Material	Cu	Al	Ni	Ti	Mild Steel	Zn
Density ρ_p, Kgm^{-3}	8960	2710	8890	4510	7870	7140 6660
Thermal conductivity K	386	220				
Specific Heat C_p, $J(Kg^oC)^{-1}$	383	920	456	528	481	
Heat of Fusion $J(kg)^{-1}$	207 000	321 000				
Melting Point K	1356	916	1726	1923	1793	
Elastic Modulus GPa	124	68.9	207	116	200.1	108
Poisson's ratio	0.34	0.3	0.31	0.34	0.30	0.25
Bulk modulus GPa	140	71.7	182	110	140	70
Bulk speed of sound C_o, ms^{-1}	3952.8	5143.7	4524.6	4938.6	4217.7	3131.1 3256.7
J C Plasticity A, B,MPa, n, C, m	90, 292 0.31,0.025,1.09	148				

Table 1: Properties of copper (Johnson and Cook, 1985), Aluminum (Gupta et al., 2006), Nickel (Razavipour and Jodoin, 2021), Titanium, Mild Steel (Bae et al., 2008)

3 Results and Discussion

3.1 Plastic strain rate in the substrate interfacial material

In order to model this problem, let γ_s be the energy transferred to the substrate and used in plastic deformation from initial energy of the impacting particle. Then from the kinetic energy of the particle the plastic deformation energy will be given by

$$\gamma_s \times \frac{1}{2}\rho_p V_{n_p} {v_p}^2 = \sigma_{y_s}\left(\frac{d\varepsilon_p}{dt}.t_c\right) V_{pl_s} \tag{5}$$

Isolation of impact velocity yields equation 6

$$v_p = \left(\frac{2\times\sigma_{y_s}\times\dot{\varepsilon}_s.t_c\times V_{pl_s}}{\gamma_s\times\rho_p V_{n_p}}\right)^{1/2} \tag{6}$$

Since around the critical velocity, $t_c \approx d_p/v_p$, see for instance in Hassani-Gangaraj et al. (2018b) and Maev and Leshchynsky (2009), hence equation 6 can be written as

$$v_p \approx \left(\frac{2\times\sigma_{y_s}\times(\dot{\varepsilon}.d_p)\times V_{pl_s}}{\gamma_s\times\rho_p V_{n_p} v_p}\right)^{1/2} \tag{7}$$

Let $\mu_s = 2\times V_{pl_s}/((V_{n_p}))$, then equation 7 can be given as

$$v_{cr} \approx \left(\frac{\sigma_{y_s}\times(\dot{\varepsilon}_s.d_p)\,\mu_s)}{\gamma_s\rho_p}\right)^{1/3} \tag{8}$$

defining the critical velocity for adhesion.

Previous studies have pointed out the relation of critical speed of adhesion to the bulk speed of sound in the material. At the critical velocity of adhesion, $\dot{\varepsilon}_s.d_p\mu_s$ should relate to the bulk speed of sound C_s, and v_p is equal to v_{cr}. It is important to take note that here the variables used are the nominal variables involving an undeformed particle volume. The variations in the density and the elasticity of the particle through Poisson's ratio due to elasticity and deformation may determine the exact location. To further substantiate this claim, equation 8 is further analysed in Figure 2 using the non-dimensional values which gives a characterization of the nano scale structural dynamics. The lower bound is defined by the response variable C_o/v_p and the upper bound for erosion by $(C_o/v_p)^2$, severity of impact is given by $(\gamma_s\rho_p v_p^2)/(\sigma_{y_s})$ where γ_s is given as 1/2 as an approximation (γ_s at critical was numerically observed to be higher than γ_p). The assertion that $\dot{\varepsilon}_s.d_p\mu_s$ relates to C_s at the critical velocity, brings a new discourse to a consideration of the internal structural dynamics during this process. The results of which may inform experimental

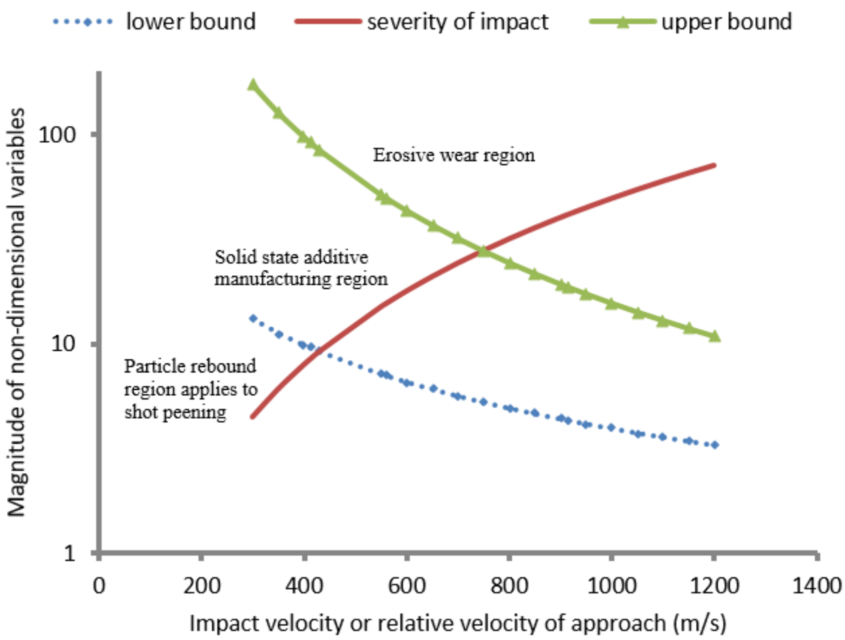

Figure 2: Critical and erosion velocity equations for adhesion of microparticles on a substrate surface.

interrogation methods for the transient impact dynamic state. On the plasticity of the material, since the plastic equivalent strain, can be estimated from $((\gamma_s \rho_p {v_p}^2))/\sigma_{y_s} = 2 \times (\varepsilon_{pl})(V_{pl_s}/V_{n_p})$, it seems for some materials the spall strength of the substrate could be estimated from σ_{y_s}/γ_s a similar argument can be made about the particle. The limitation is that σ_{y_s} used in this analysis is a quasi-static value of the material plasticity at room temperature. Thermal softening would lower the dynamic yielding to zero in the material model at melting, see the Johnson cook equation Johnson and Cook (1983). A comparison on these values can be made between various materials for instance between Cu and Al to see how this value, σ_{y_s}/γ_s, would relate to the spall strength.

In a numerical analysis, data was obtained from the impact simulations of a 10µm diameter copper particle on copper substrate with material properties listed in Table 1. For the impact velocity of $412.6ms^{-1}$, the maximum plastic equivalent strain was recorded, the plastic energy in the particle, and the plastic energy in the substrate. The parameters estimated in the computational analysis are shown in equation 9.

$$v_p = \left(\frac{2 \times \sigma_{y_s}}{\rho_p} \left(\frac{\varepsilon_{Pl}}{\gamma_s} \right) \left(\frac{V_{pl_s}}{V_{n_p}} \right) \right)^{1/2} \tag{9}$$

From the energy balance γ_s was 0.564 and γ_p was 0.291, where γ_s was the ratio of plastic energy in the substrate to the kinetic energy of the particle and γ_p was the ratio of plastic energy in the particle to the kinetic energy of the particle. The total plastic energy $\alpha_{pl} = \gamma_s + \gamma_p$ is the ratio amount of kinetic energy used in the plastic straining of both the particle and the substrate. The volume ratio V_{pl_s}/V_{n_p} was 1.463, plastic equivalent strain ε_{pl} was 3.263 plastic energy in substrate $2.25x10^{-7}J$, plastic energy in the particle $1.16x10^{-7}J$. This data was all based on numerical simulations. The plastic affected volume in the substrate was calculated from the following equation: $E_{pl_s} = \sigma_{y_s}(\varepsilon_p l)V_{pl_s}$, where E_{pl_s} is the numerically calculated plastic energy in the substrate, ε_{pl} was set to the maximum plastic equivalent strain.

3.2 Interfacial temperature increase in a single particle impact

Now we move from the plastic deformation to the heat generation. For heat generation rate in the substrate interfacial material an additional parameter $\beta = 0.9$ heat conversion parameter is added. Below the melting temperature, the change in temperature at the interface ΔT in the substrate can be accounted for as

$$\Delta T = \frac{\beta \varepsilon_{p_s} \sigma_{y_s} V_{pl_s}}{\rho c_{p_s} V_{th_s}} \tag{10}$$

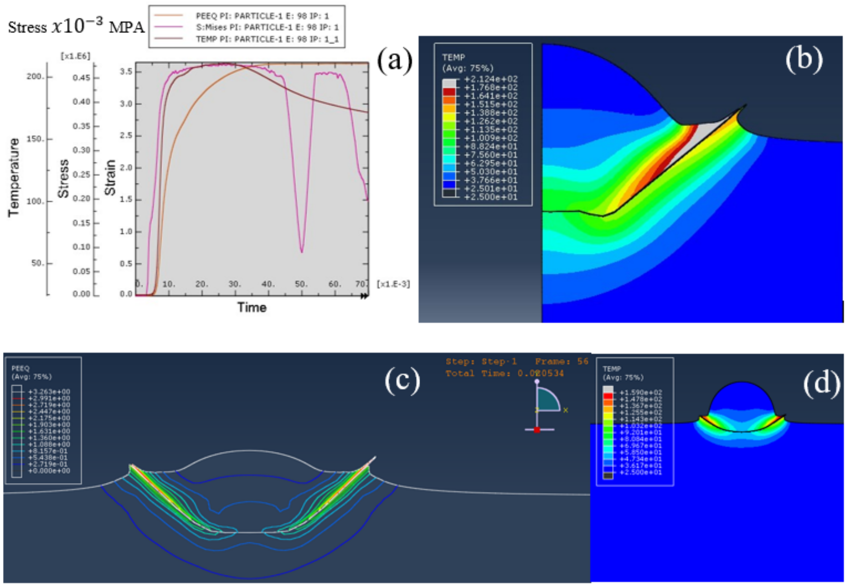

Figure 3: (a) shows the temporal evolution of temperature, stress and strain and (b) typical temperature values from the simulations at 500 ms^{-1}, of a 20μm Cu particle impacting a Cu substrate in a non-adiabatic analysis. The image in (c) gives the plastic equivalent strain and (d) typical temperature values from the simulations at 412.6 ms^{-1} impact of a 10μm diameter Cu particle impacting a Cu substrate in a non-adiabatic analysis (all temperatures in degree Celsius, initial temperature was 25 degrees Celsius).

Where V_{pl_s} is the plastic affected volume, and V_{th_s} thermal heating affected volume and other parameters as previously defined. The plastic strain ε_{p_s} is velocity dependent and is also dependent of the assumption of adiabatic or non-adiabatic heat transfer. See equation 9 for the details on the plastic equivalent strain as detailed in the previous section. The yield stress used in equation 9 is obtained from the Johnson cook model material parameters, for instance $90MPa$ for copper, Table 1. With adiabatic modelling, the change in temperature at the critical velocity is much higher than for non-adiabatic analysis. In this section examples of temperature evolution and plastic equivalent strains studied for the non-adiabatic solution are shown in Figure 3. From the simulations at $412.6ms^{-1}$ impact of a $10\mu m$ diameter Cu particle impacting a Cu substrate in a non-adiabatic analysis the maximum plastic equivalent strain attained was 3.263 at $20.5ns$ after impact; the maximum temperature was 159 degrees Celsius at $7.33ns$ after impact. The other issue is that of thermal resistance at the interface, this value is normally not known in continuum computational studies. In Figure 3 interfacial jetting as seen induces tensile stresses, an analysis of these are reported in (Moonga and Jen, 2017).

3.2.1 Interfacial Melting and Erosion velocity in relation to the critical velocity

A similar approach as from the previous sections is used here. Let γ_s be the ratio of the kinetic energy used in plastic deformation of the substrate. Then from the initial kinetic energy of the particle

$$\beta \times \gamma_s \times 1/2\rho_p V_{n_p} v_e^2 = \rho_s V_{th_s}[C_{p_s}(T_{m_s} - T_o) + H_{f_s}] \tag{11}$$

Here β is the tailor quinney constant which accounts for amount of plastic strain converted to heat,γ_s is the amount of plastic strain energy in the substrate with reference to the initial kinetic energy of the particle. H_{f_s} is the heat of fusion, T_o is the room temperature, T_m the melting temperature, C_p the specific heat capacity, V_{th} is the affected volume in the substrate around the interface, ρ_p is the density of the particle material, ρ_s is the density of the substrate material, d_p is the particle diameter, v_e is the impact velocity at onset of erosion; V_{th} is the thermal heating affected volume in the substrate and can be written as $V_{th} = A_c\, d_{th}$ here A_c is the contact area between the substrate and the deformed particle; d_{th} is the thermal depth. From equation 11

$$v_e = \left(\frac{2\rho_s V_{th_s}[C_{p_s}(T_{m_s} - T_o) + H_{f_s}]}{\gamma_s \beta \rho_p V_{n_p}} \right)^{1/2} \tag{12}$$

For an approximate solution, here the contact area and thermal depth have previously been estimated in (Hassani-Gangaraj et al., 2018b) as $A_c = \pi d_p^2/2$, $d_{th} = (k_s/(\rho_s C_s) \times t_c)^{1/2}$ where k_s is the thermal conductivity, t_c is the time of contact between the substrate and the particle. For a numerical example, assuming Cu; with $d_p = 15$micron, $A_c = 3.534 \times 10^{-10} m^2$, $d_{th} = 1.341 \mu m$; let $\gamma_s = 0.5$, $\beta = 0.9$, and $H_{f_s} = 207000 J/kg$. The erosion velocity can now be calculated considering the nonzero heat of fusion as giving an erosion velocity v_e of $854.2 ms^{-1}$ with similar results as obtained by (Hassani-Gangaraj et al., 2018b).

In the computational studies we conducted in trying to understand the thermal model, strain value has been observed to depend on adiabatic or non-adiabatic conditions and initial temperatures. Equation 6 through to equation 12 and dynamic relations given in Figure 2 can be summarised, in the first part, for onset of erosion to be governed by the equation 13

$$\frac{\gamma_{s_e} \rho_p v_e^2}{\sigma_{y_s}} \frac{V_{n_p}}{V_{th_s}} = b \left(\frac{C_o}{v_e} \right)^2 \left(\frac{V_{pl_s}}{V_{th_s}} \right) = 2 \times \varepsilon_{pl} \left(\frac{V_{pl_s}}{V_{th_s}} \right) = \frac{\rho_s [C_{p_s} (T_{m_s} - T_o) + H_{(f_s)}]}{\beta \sigma_{y_s}} \tag{13}$$

and in the second part, onset of adhesion to be governed by equation 14 where T_{cr_s} is the substrate temperature at the critical velocity.

$$\frac{\gamma_{s_{cr}} \rho_p v_{cr}^2}{\sigma_{y_s}} \left(\frac{V_{n_p}}{V_{th_s}} \right) = a \left(\frac{C_o}{v_{cr}} \right) \left(\frac{V_{pl_s}}{V_{th_s}} \right) = (2 \times \varepsilon_{pl}) \left(\frac{V_{pl_s}}{V_{th_s}} \right) = \frac{\rho_s [C_{p_s} (T_{cr_s} - T_o)]}{\beta \sigma_{y_s}}. \tag{14}$$

Equation 13 and equation 14 can be considered to be the nominal equations where the underlying dynamics that govern rebound, adhesion and erosion can be traced. It should be interesting to see how this result relates to higher speed shock velocities such as these (Stewart et al., 2023; Ma et al., 2020; Guo et al., 2024). The development of experimental in-situ observations of micro particle impact velocity and rebounding velocity reported in (Hassani-Gangaraj et al., 2018b; Reiser and Schuh, 2023) provided more insight on this problem. In-situ observation of interfacial temperature evolutions at these length scales and time scales has been difficult (Chaban et al., 2021), as this would require ultrafast thermal measurement processes. Another area that would make significant contribution is that of the acoustics and vibrational measurements; but has not yet been explored for this problem. Plastic strain measurements in ultrafast experimental processes are normally used to determine the dynamic yield stress, and these normally use larger specimens, and the interest is normally not the transient dynamics of the deformation process leading to adhesion or rebound. Whilst the idea of interfacial jetting by hydrodynamic pressure had been proposed previously (Hassani-Gangaraj et al., 2018b), the relations given in the forgoing equations point to the fundamental physics.

4 Proposed future directions

4.1 Microscopic heat transfer

The need for increased understanding of the energy transport mechanisms at small length scales gave rise to the field of microscale heat transfer which involves study of individual heat carriers (Bejan and Kraus, 2003). Microscale heat transfer can be considered when the continuum model is nolonger valid at small length scales or small time scales compared to the intrinsic properties of the heat carriers. In the classical continuum model the heat transfer analysis applies the conservation of energy equation 3 coupled with Fourier's law for thermal conduction in the solution procedures. The first attempt at microscale heat transfer modeling is to modify the continuum model in such a way to account for microscale thermal transport relations. One common approach, though difficult, applies the Boltzmann transport equation. When both these methods fail, molecular dynamics can be adopted. Microscopic heat transfer analysis requires analyzing microscopic energy carriers and the basic heat transfer mechanism (Bejan and Kraus, 2003). The basic thermal carriers in metals are the free electrons, while in semiconductors and insulators are the lattice vibrations (phonons) which travel like acoustic waves. Theoretical descriptions of electrons and phonons are based on the assumption that the material is of crystalline structure (Bejan and Kraus, 2003).

In microscopic analysis, Catteneo's equation 15 can be used to account for finite speed of thermal energy propagation (Bejan and Kraus, 2003).

$$\frac{1}{\tau} \frac{\partial q}{\partial t} + q = \frac{-K}{\Delta T} \tag{15}$$

where τ is the relaxation time of the heat carrier. Substitution into the conservation equation gives a hyperbolic differential equation. Equation 15 reduces to Fourier's law when relaxation time is much less than the time scales of interest. At present it's not yet clear whether during high speed impacts the interfacial temperatures are properly defined using adiabatic analysis or using non adiabatic analysis where heat flow through conduction is accounted using Fourier's law. It could be that a better estimate of the heat transport could be made through equation 15. This equation would account for the time delay for the heat flux to develop after temperature gradient has been applied.

4.2 Vibrations and acoustics

Micro and nano particle vibrational signatures (Tang et al., 2023); and wave propagation mechanism (Karman and Duwez, 1950) in the particle will definitely inform on the underlying dynamics pointed to by the equations and methods defined in this report, especially in relation to high strain rate deformation.

5 Conclusion

There is an observed relationship between plastic strain rates and acoustics in the impacting particle by illustrative underlying dynamics that may lead to rebound, bonding or erosive wear. The window of deposition was thus defined by the critical and erosion velocities defined by continuum material parameters. Varying these parameters would therefore vary the location of the critical and erosion velocities, shifting the erosion or deposition window. It should be possible also to vary the width of the deposition window. At this point it was not conclusive of the heat transport across the particle substrate interface, this requires some further examination. The heat generation and thermal analysis at the interface should be able to provide a connection to plastic strains, plastic strain rates and energy distribution after impact. The levels of temperatures attained will definitely provide more details to the adhesion energy, and the strength of the bonding. This analysis should be able to give better connection to the underlying dynamics. Bonding is an interfacial process whilst rebound is based on the bulk of the particles recoverable energy in interaction with the substrates recoverable energy. Adhesion delay has been observed experimentally; where the first particles rebound however once the surface chemistry has changed bonding takes off, indicating the importance of interfacial physics in bonding. This study advances the understanding on the high strain deformation during micro particle impacts.

References

Al-Obaid, Y. F. (1995). Shot peening mechanics: experimental and theoretical analysis. *Mechanics of Materials*, ISBN: 01676636, ISSN: 01676636, DOI: 10.1016/0167-6636(94)00036-G.

Alkhimov, A. P., Papyrin, A. N., Kosarev, V. F., Nesterovich, N. I., and Shushpanov, M. M. (1994). Gas dynamic spraying method for applying a coating. ISBN: 3077465469, DOI: U.S. Patent 5,302,414;.

Bae, G., Xiong, Y., Kumar, S., Kang, K., and Lee, C. (2008). General aspects of interface bonding in kinetic sprayed coatings. *Acta Materialia*, 56:4858–4868, ISBN: 1359-6454, ISSN: 13596454, DOI: 10.1016/j.actamat.2008.06.003.

Bejan, A. and Kraus, A. D. (2003). *Heat transfer handbook*, volume 1. John Wiley & Sons, ISBN: 0471390151, ISSN: 1520-5126, DOI: 10.1021/ja1097622.

Chaban, I., Sun, Y., Veysset, D., Nelson, K. A., and Schuh, C. A. (2021). The effect of substrate temperature on the critical velocity in microparticle impact bonding. *Applied Physics Letters*, 119, ISSN: 00036951, DOI: 10.1063/5.0055274.

Dowding, I., Hassani, M., Sun, Y., Veysset, D., Nelson, K. A., and Schuh, C. A. (2020). Particle size effects in metallic microparticle impact-bonding. *Acta Materialia*, 194:40–48, ISSN: 13596454, DOI: 10.1016/j.actamat.2020.04.044.

Guo, X.-X., Jiang, D.-D., and Shao, J.-L. (2024). Atomistic simulation of structural transition and grain refinement in fe nanowires driven by high strain rate compression. *Journal of Applied Physics*, 135, ISSN: 0021-8979, DOI: 10.1063/5.0176619, https://pubs.aip.org/jap/article/135/3/035102/3000629/Atomistic-simulation-of-structural-transition-and.

Gupta, N. K., Iqbal, M. A., and Sekhon, G. S. (2006). Experimental and numerical studies on the behavior of thin aluminum plates subjected to impact by blunt- and hemispherical-nosed projectiles. *International Journal of Impact Engineering*, 32:1921–1944, ISBN: 0734743X, ISSN: 0734743X, DOI: 10.1016/j.ijimpeng.2005.06.007.

Hassani-Gangaraj, M., Veysset, D., Nelson, K. A., and Schuh, C. A. (2018a). In-situ observations of single micro-particle impact bonding. *Scripta Materialia*, 145:9–13, ISBN: 1359-6462, ISSN: 13596462, DOI: 10.1016/j.scriptamat.2017.09.042.

Hassani-Gangaraj, M., Veysset, D., Nelson, K. A., and Schuh, C. A. (2018b). Melt-driven erosion in microparticle impact. *Nature communications*, Accepted f, ISSN: 2041-1723, DOI: 10.1038/s41467-018-07509-y, http://dx.doi.org/10.1038/s41467-018-07509-y.

Johnson, G. R. and Cook, W. (1983). A constitutive model and data for metals subjected to large strains, high strain rates, and high temperatures. In *Seventh International Symposium on Ballistics*, pages 541–547.

Johnson, G. R. and Cook, W. H. (1985). Fracture characteristics of three metals subjected to various strains, strain rates, temperatures and pressures. *Engineering Fracture Mechanics*, ISBN: 0013-7944, ISSN: 00137944, DOI: 10.1016/0013-7944(85)90052-9.

Karman, T. V. and Duwez, P. (1950). The propagation of plastic deformation in solids. *Journal of Applied Physics*, 21:987–994, ISSN: 00218979, DOI: 10.1063/1.1699544.

Li, C. J., Li, W. Y., and Liao, H. (2006). Examination of the critical velocity for deposition of particles in cold spraying. *Journal of Thermal Spray Technology*, 15:212–222, ISBN: 105996306X, ISSN: 10599630, DOI: 10.1361/105996306X108093.

Ma, X., Zhao, D., Yadav, S., Sagapuram, D., and Xie, K. Y. (2020). Grain-subdivision-dominated microstructure evolution in shear bands at high rates. *Materials Research Letters*, 8:328–334, ISSN: 21663831, DOI: 10.1080/21663831.2020.1759155.

Maev, R. G. and Leshchynsky, V. (2009). *Introduction to low pressure gas dynamic spray: physics and technology*. John Wiley & Sons.

Moonga, K. and Jen, T. (2017). Residual stress characterization from numerical analysis of the multi-particle impact behavior in cold spray. In *Advanced Manufacturing*, volume 2. ISBN: 9780791858356, DOI: 10.1115/IMECE2017-71225.

Moonga, K. H. (2019). *Investigation of the Cold Gas Dynamic Spray Technique for the fabrication of a Thin Film for a Plasmonic Biosensor*. PhD thesis, University of Johannesburg.

Moridi, A., Hassani-Gangaraj, S. M., and Guagliano, M. (2013). A hybrid approach to determine critical and erosion velocities in the cold spray process. *Applied Surface Science*, 273:617–624, ISBN: 0169-4332, ISSN: 01694332, DOI: 10.1016/j.apsusc.2013.02.089, http://dx.doi.org/10.1016/j.apsusc.2013.02.089.

Palmieri, D. and Lambert, M. (2001). Prediction of impact damage on double bumper shields for the protection of orbiting manned modules. In *3rd European Conference on Space Debris*. ESA, https://conference.sdo.esoc.esa.int/proceedings/sdc3/paper/36.

Rahmati, S. and Ghaei, A. (2014). The use of particle/substrate material models in simulation of cold-gas dynamic-spray process. *Journal of Thermal Spray Technology*, 23:530–540, ISBN: 8415683111, ISSN: 10599630, DOI: 10.1007/s11666-013-0051-4.

Razavipour, M. and Jodoin, B. (2021). Material model for predicting dynamic response of copper and nickel at very high strain rates under cold spray conditions. *Journal of Thermal Spray Technology*, 30:324–343, ISSN: 15441016, DOI: 10.1007/s11666-020-01137-z.

Reiser, A. and Schuh, C. A. (2023). Microparticle impact testing at high precision, higher temperatures, and with lithographically patterned projectiles. *Small Methods*, 7, ISSN: 23669608, DOI: 10.1002/smtd.202201028.

Schmidt, T., Gärtner, F., Assadi, H., and Kreye, H. (2006). Development of a generalized parameter window for cold spray deposition. *Acta Materialia*, 54:729–742, ISBN: 1359-6454, ISSN: 13596454, DOI: 10.1016/j.actamat.2005.10.005.

Simulia, D. S. (2012). Analysis user's manual volume 2: Analysis. *Abaqus 6.12*, II.

Stewart, J. A., Startt, J. K., and Dingreville, R. (2023). A molecular dynamics study on the mie-grüneisen equation-of-state and high strain-rate behavior of equiatomic cocrfemnni. *Materials Research Letters*, 11:1055–1062, ISSN: 21663831, DOI: 10.1080/21663831.2023.2280635.

Tang, S.-J., Zhang, M., Sun, J., Meng, J.-W., Xiong, X., Gong, Q., Jin, D., Yang, Q.-F., and Xiao, Y.-F. (2023). Single-particle vibrational spectroscopy using optical microresonators. *Nature Photonics*, 17:951–956, DOI: 10.1038/s41566-023-01264-3.

Wang, Q., Ma, N., Huang, W., Shi, J., Luo, X. T., Tomitaka, S., Morooka, S., and Watanabe, M. (2023). Key role of temperature on delamination in solid-state additive manufacturing via supersonic impact. *Materials Research Letters*, 11:742–748, ISSN: 21663831, DOI: 10.1080/21663831.2023.2227221.